Atmospheric
Chemistry
and Physics
Discussions

Open Access

EGU

# Responses of Arctic Black Carbon and Surface Temperature to Multi-Region Emission Reductions: an HTAP2 Ensemble Modeling Study

**Na Zhao[1], Xinyi Dong[2], Joshua S. Fu[3,4*], Marianne Tronstad Lund[5], Kengo Sudo[6], Daven Henze[7], Tom Kucsera[8], Yun Fat Lam[9], Mian Chin[10], Simone Tilmes[11], Kan Huang[1]***

[1] Shanghai Key Laboratory of Atmospheric Particle Pollution and Prevention (LAP3), Department of Environmental Science and Engineering, Fudan University, Shanghai, China

[2] School of Atmospheric Science, Nanjing University, Nanjing, China

[3] Department of Civil and Environmental Engineering, The University of Tennessee, Knoxville, Tennessee, USA

[4] Computational Earth Science Group, Computational Sciences and Engineering Division, Oak Ridge National Laboratory, Oak Ridge, Tennessee, USA

[5] CICERO Center for International Climate and Environmental Research, Oslo, Norway

[6] Nagoya University, Furo-cho, Chigusa-ku, Nagoya, Japan

[7] Department of Mechanical Engineering, University of Colorado, Boulder, CO, USA

[8] Universities Space Research Association, Greenbelt, MD, USA

[9] Department of Geography, The University of Hong Kong, HKSAR, China

[10] Earth Sciences Division, NASA Goddard Space Flight Center, Greenbelt, MD, USA

[11] Atmospheric Chemistry Observations and Modeling Laboratory, National Center for Atmospheric Research, Boulder, Colorado, USA

Correspondence: jsfu@utk.edu; huangkan@fudan.edu.cn

## ABSTRACT

Black carbon (BC) emissions play an important role in regional climate change of the Arctic. It is necessary to pay attention to the impact of long-range transport from regions outside the Arctic as BC emissions from local sources in the Arctic were relatively small. The Task Force Hemispheric Transport of Air Pollution Phase2 (HTAP2) set up a series of simulation scenarios to investigate the response of BC in a given region to different source regions. This study investigated the responses of Arctic BC concentrations and surface temperature to 20% anthropogenic emission reductions from six regions in 2010 within the framework of HTAP2 based on ensemble modeling results. It was found that the emissions from East Asia (EAS) had most (18.1%–51.4%) significant impact on the Arctic

36    while the monthly contributions from Europe, Middle East, North America, Russia Belarus Ukraine,

37    and South Asia were 20.1%–49.9%, 0.02%–0.9%, 8.3%–19.3%, 5.4%–18.1%, and 3.1%–7.7%,

38    respectively. The responses of the vertical profiles of the Arctic BC to the six regions were found to be

39    different due to multiple transport pathways. The response of the Arctic BC to emission reductions of

40    six source regions became less significant with the increase of the latitude. The benefit of BC emission

41    reductions in terms of slowing down surface warming in the Arctic was evaluated by using Absolute

42    Regional Temperature-change Potential (ARTP). Compared to the response of global temperature to

43    BC emission reductions, the response of Arctic temperature was substantially more sensitive,

44    highlighting the need for curbing global BC emissions.


45    **1. Introduction**


46    Black carbon (BC) is one of the short-lived climate forcers (SLCFs, AMAP, 2015) and was regarded

47    as the second largest contributor to global warming, only inferior to carbon dioxide (Bond et al. 2013).

48    BC over the Arctic can perturb the radiation balance in a number of ways. Direct aerosol forcing

49    occurred through absorption or scattering of solar (shortwave) radiation. BC is the most efficient

50    atmospheric particulate species at absorbing visible light (Bond et al. 2013), the added atmospheric

51    heating will subsequently increase the downward longwave radiation to the surface and warm the

52    surface (AMAP, 2011). Radiative forcing by BC can also result from aerosol-cloud interactions that

53    affected cloud microphysical properties, albedo, extent, lifetime, and longwave emissivity (Twomey

54    1977; Garrett and Zhao 2006). BC has an additional forcing mechanism after depositing onto snow

55    and ice surfaces (Clarke and Noone, 1985). The surface albedo of snow and ice could be reduced and

56    further enhanced the absorption of solar radiation at the surface. In the Arctic, surface temperature

57    responses were strongly linked to surface radiative forcing as the stable atmosphere of the region

58    prevented rapid heat exchange with the upper troposphere (Hansen and Nazarenko, 2004).

59    The Arctic has been warming twice as rapidly as the world in the past fifty years, and has

60    experienced significant changes in its ice and snow covers as well as permafrost (AMAP, 2017).

61    Reductions of carbon dioxide emissions are the backbone of any meaningful effort to mitigate climate

62    forcing. But even if significant reductions of carbon dioxide are made, slow down of the temperature

63    rise in the Arctic and the sea level rise caused by the melting of glaciers may not be achieved in time.

64     Hence, the goal of slowing down the deterioration of the Arctic may best be achieved by also targeting

65     at shorter-lived climate forcing agents, especially those that could impose appreciable surface forcing

66     and trigger regional-scale climate feedbacks pertaining to the melting of sea ice and snow. Modelling

67     studies by UNEP/WMO (2011) and Stohl et al. (2015) suggested that the climate response of SLCFs

68     mitigation was strongest in the Arctic region. AMAP (2011 and 2015) as well as Sand et al. (2016)

69     demonstrated that per unit of emission reductions of SLCFs in the Northern areas had the largest

70     temperature response on the Arctic, with the Nordic countries (Denmark, Finland, Iceland, Norway,

71     and Sweden) and Russia having the largest impact compared to other Arctic countries such as the

72     United States and Canada.

73         The few studies that investigated specific regional aerosol forcing (Shindell and Faluvegi, 2009;

74     Shindell et al., 2012; Teng et al., 2012) typically used a single climate model at a time to investigate

75     the climate response to idealized, historical, or projected forcing. However, different models varied

76     considerably in the representation of aerosols and radiative properties, resulting in large uncertainties

77     in simulating the aerosol radiative forcing (Myhre et al., 2013b; Shindell et al., 2013). When

78     investigating the climate response to regional emissions, such uncertainties were likely to be

79     confounded even further by the variability between models in regional climate and circulation patterns

80     and variation in the global and regional climate sensitivity (the amount of simulated warming per unit

81     radiative forcing). Hence, the Task Force Hemispheric Transport of Air pollution Phase2 (HTAP2,

82     http://www.htap.org/) incorporating multiple global models can avoid the great uncertainty of single

83     model to a certain degree, with the aim to improve model estimates of the impacts of intercontinental

84     transport of air pollutants on climate, ecosystems, and human health (Galmarini et al., 2017). To date,

85     the HTAP2 results have been explored from a variety of scientific and policy-relevant perspectives.

86     For instance, by comparing against observations, sulfur and nitrogen depositions during HTAP2 had

87     been significantly improved compared to HTAP1. From 2001 to 2010, the global nitrogen deposition

88     increased 7% while the global sulfur deposition decreased 3% (Tan et al., 2018a). The significant

89     impacts of hemispheric transport on the deposition were specifically focused and the deposition over

90     the coastal regions was more sensitive to hemispheric transport than the non-coastal continental

91     regions (Tan et al., 2018b). Jonson et al. (2018) assessed the contributions from different world regions

92     to European ozone levels and contributions from the non-European regions were mostly from North

93   America and eastern Asia, larger than those from European emissions. Hogrefe et al. (2018) found that

94   the simulated ozone over the continental US varied very differently by digesting boundary conditions

95   from four hemispheric or global models. The impact of emission changes from six major source

96   regions on global aerosol direct radiative forcing was estimated (Stjern et al., 2016). In the local source

97   regions, the radiative forcing associated with $SO_4^{2-}$ was strengthened (25%) while that from BC was

98   weakened (37%) due to a 20% emission reduction. Liang et al. (2018) estimated global air-pollution-

99   related premature mortality from exposure to $PM_{2.5}$ and ozone and the interregional transport lead to

100  more deaths through changes in $PM_{2.5}$ than in $O_3$. However, the source region contributions to Arctic

101  BC and the spread among multi-model results have been rarely explored from the perspective of

102  HTAP2 initiative.

103  This study aims to investigate the responses of Arctic BC concentrations and surface temperature to

104  20% anthropogenic emission reductions from different regions in the Northern Hemisphere. A

105  comparison of six global modeling works within the framework of HTAP2 experiments for the Arctic

106  region in 2010 was presented. The ensemble modeling results were used to apportion the contribution

107  from different source regions to the near-surface and vertical black carbon in the Arctic. In addition,

108  the Arctic surface temperature responses to the emission reductions were estimated.

109  **2. Methodology**

110  **2.1 HTAP2 experiments**

111  HTAP2 developed a harmonized emissions database covering all countries and the major sectors for

112  global and regional modeling from 2008 to 2010. The emissions database was obtained from the

113  nationally reported emissions (e.g., National Emission Inventory for the United States), the regional

114  scientific inventories (e.g., Model Inter-Comparison Study for Asia, MICS–Asia III), and the

115  Emissions Database for Global Atmospheric Research data (EDGARv4.3, emissions for South

116  America, Africa, Russia and Oceania). Biomass burning emissions were not prescribed in HTAP2. It

117  was recommended that modeling groups used the Global Fire Emissions Database (GFED4,

118  http://globalfiredata.org/) with a temporal resolution of daily or 3–hour intervals. The detailed

119  information of different regional inventories can be found in (Janssens–Maenhout et al., 2015).

120    Emission perturbations were conducted in sensitivity simulations to investigate the response of

121    various air pollutants in a given region to different source regions. In this study, the Arctic region was

122    the targeted receptor region of interest. Six source regions in HTAP2 experiments, namely, East Asia

123    (EAS), Europe (EUR), Middle East (MDE), North America (NAM), Russia–Belarus–Ukraine (RBU),

124    and South Asia (SAS) were selected to demonstrate their influences on the BC concentrations over the

125    Arctic region (Figure 1a). Two emission scenarios were designed for the HTAP2 simulation to explore

126    the source/receptor relationships, i.e. the base scenario (BASE) with no emission reduction, and the

127    control scenario (EASALL, EURALL, MDEALL, NAMALL, RBUALL, and SASALL) with 20%

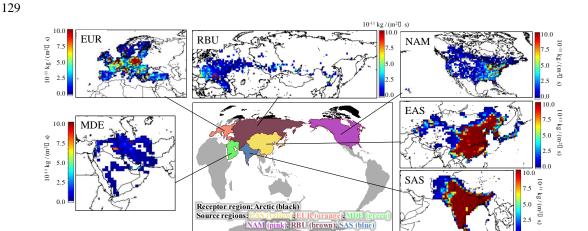128    reduction of all anthropogenic emissions in six regions, respectively.

129



130

131    **Figure 1. (a)** The sketch map of receptor and source regions. **(b)–(g)** Spatial distributions of 20% reduction of annual

132    BC emission in the six source regions in 2010. EAS: East Asia; EUR: Europe; MDE: Middle East; NAM: North

133    America; RBU: Russia–Belarus–Ukraine; SAS: South Asia. The unit legends from (b) to (g) are the same of $10^{-11}$

134    kg (m$^2$ s)$^{-1}$.

135    **2.1.1 Anthropogenic emission reductions of BC in HTAP2**

136    Anthropogenic BC emission sectors included power plants, industries, transportation, shipping,

137    aviation, agriculture, and residential sectors. The emission inventory had a monthly temporal

138    resolution and a spatial resolution of $0.1° \times 0.1°$. The total anthropogenic emissions and 20% emission

139    reductions of BC in six source regions of HTAP2 in 2010 are presented in Table 1. The higher BC

140    emission reductions were found in EAS and SAS with the values of 355.6 and 232.5 Gg yr$^{-1}$,

141    respectively, while were much lower in MDE and RBU with the values of 5.3 and 18.6 Gg yr$^{-1}$,

142    respectively. The BC emission reductions in EAS, EUR, and RBU indicated significant monthly

143    variations with higher values from November to March, while the monthly variations were not obvious

144    in MDE, NAM, and SAS.

145

146    **Table 1.** 20% emission reductions and total anthropogenic emissions of BC in different regions of HTAP2 in 2010.

147    (Unit: Gg yr$^{-1}$).

| Regions | Total anthropogenic emissions | 20% Emission Reductions | | | | | | | | | | | |
|---|---|---|---|---|---|---|---|---|---|---|---|---|---|
| | | Feb | Mar | Apr | May | Jun | Jul | Aug | Sep | Oct | Nov | Dec | All |
| EAS[a] | 1778.1 | 35.6 | 33.0 | 24.1 | 23.9 | 24.0 | 24.0 | 23.6 | 23.5 | 25.0 | 31.4 | 41.0 | 355.6 |
| EUR[b] | 326.3 | 6.4 | 7.2 | 6.5 | 5.3 | 4.9 | 4.0 | 3.7 | 4.4 | 5.2 | 5.3 | 5.7 | 65.3 |
| MDE[c] | 26.7 | 0.4 | 0.5 | 0.5 | 0.5 | 0.4 | 0.4 | 0.4 | 0.4 | 0.5 | 0.5 | 0.5 | 5.3 |
| NAM[d] | 310.8 | 5.1 | 5.3 | 5.1 | 5.1 | 5.2 | 5.3 | 5.3 | 5.1 | 5.1 | 5.1 | 5.2 | 62.2 |
| RBU[e] | 93.0 | 1.9 | 1.9 | 1.7 | 1.4 | 1.3 | 1.0 | 1.1 | 1.2 | 1.6 | 1.7 | 1.8 | 18.6 |
| SAS[f] | 1162.7 | 19.1 | 19.7 | 18.9 | 19.2 | 18.9 | 19.2 | 19.2 | 19.0 | 19.3 | 19.2 | 20.4 | 232.5 |
| All | 3697.6 | 68.5 | 67.6 | 56.8 | 55.4 | 54.7 | 53.9 | 53.3 | 53.6 | 56.7 | 63.2 | 74.6 | 739.5 |

148    [a] East Asia. [b] Europe. [c] Middle East. [d] North America. [e] Russia–Belarus–Ukraine. [f] South Asia.

149

150    Figure 1b–g illustrates the spatial distribution of the 20% reductions of annual BC emissions in six

151    source regions in 2010. It can be found that the most intense reductions of BC emissions in EAS and

152    SAS were concentrated in East China and India, respectively, which were mainly attributed to

153    emissions from residential sectors, followed by transportation and industries. The BC emission

154    reductions of EUR were widely distributed with high values in central Europe, with residential and

155    transportation sectors accounting for the largest proportions. The reductions near the Arctic circle could

156    be found in the north of EUR, NAM, and RBU. For MDE, most BC was emitted from Iran, which

157    located in the northeast of this region. Overall, the spatial pattern of BC emission reductions in six

158    regions was closely related to the distribution of human populations.

159

160    **2.1.2 Model description**

161    In this study, six global models (CAMchem, CHASER_re1, CHASER_t106, GEOS-Chem,

162    GOCART–v5, and OsloCTM3–v2) in BC experiment were incorporated to simulate the responses of

Atmospheric
Chemistry
and Physics
Discussions
Open Access
EGU

163  BC concentrations in the Arctic to 20% BC emission reductions of the EAS, EUR, MDE, NAM, RBU,

164  and SAS, respectively. The brief information of model configurations is listed in Table 2. As required

165  by HTAP2, all simulations should include a spin-up time of 6 months prior to the period of interest.

166  The outputs from all models are available upon request from http://aerocom.met.no. The time

167  resolution of the outputs used in this study is monthly for all models, although models were run at a

168  finer resolution (e.g., daily or hourly). The model outputs for air pollutants were originally provided

169  in the unit of mass mixing ratio (MMR, kg kg$^{-1}$). To facilitate comparison between model and

170  observation and further data analysis, we converted the original units into ng m$^{-3}$ based on the ideal

171  gas law (Aamaas et al., 2017).

172

173  **Table 2.** Configurations of models used in this study

| Models | Meteorological field | Horizontal resolution | Vertical layers | Convection | Reference |
|---|---|---|---|---|---|
| CAMchem | GEOS5 v5.2 | 1.9° × 2.5° | 56 | Zhang–McFarlane approach for deep convection | Lamarque et al., 2012; Tilmes et al., 2016 |
| CHASER_re1 | ERA-Interim and HadISST | 2.8° × 2.8° | 32 | CCSR/NIES AGCM for advection, convection, and other subgrid–scale mixing | Sudo et al., 2002; Takashi et al., 2018 |
| CHASER_t106 | ERA-Interim and HadISST | 1.1° × 1.1° | 32 | CCSR/NIES AGCM for advection, convection, and other subgrid–scale mixing | Sudo et al., 2002; Takashi et al., 2018 |
| GEOS-Chem | GEOS–5 (MERRA) | 2.0° × 2.5° | 47 | Convective transport is computed from the convective mass fluxes in the meteorological archive | Henze et al., 2007 |
| GOCART–v5 | MERRA | 1.3° × 1.0° | 72 | MERRA for moist convection, Arakawa–Schubert (RAS) algorithm for GCTM | Chin et al., 2000 |
| OsloCTM3–v2 | ECMWF–IFS | 2.8° × 2.8° | 60 | Tiedke mass flux scheme for deep convection | Søvde et al., 2012; Lund et al., 2018 |

174

175  **2.2 Calculation of the temperature response to BC emissions reduction**

176  The climate effects of air pollutants have been the focus of climate change research since the last

177  century (IPCC, 1990; IPCC, 2001). In the last few years, the metrics for estimating this kind of effect

178  have been constantly improving (Shindell et al., 2012; Bond et al., 2013; Smith and Mizrahi, 2013;

179    Stohl et al., 2015). The Intergovernmental Panel on Climate Change (IPCC) used the Global Warming

180    Potential (GWP) as a method for comparing the potential climate impact of emissions of different

181    greenhouse gases (IPCC, 1990). GWP is the time-integrated radiative forcing due to a pulse emission

182    of a given species, over some given time horizon (commonly 20, 100, or 500 years) relative to a pulse

183    emission of carbon dioxide. GWP does not purport to represent the impact of air pollutant emissions

184    on temperature. Although a short-lived climate pollutant (SLCP) could have the same GWP as a long-

185    lived climate pollutant, identical (in mass terms) pulse emissions could cause a different temperature

186    change at a given time, because long-lived climate pollutants accumulate in the climate system while

187    short-lived climate pollutants can be broken down by various processes. Consequently, warming

188    caused by long-lived climate pollutants is determined by total cumulative emissions to date, while the

189    warming due to short-lived climate pollutants is determined more by the current rate of emissions in

190    any given decade and depends much less on historical emissions. This means the importance of SLCP

191    emissions is often overstated based on GWP. Shine et al. (2005) proposed the Global Temperature

192    Change Potential (GTP) as a replacement for GWP to represent the global-mean surface temperature

193    change for both a pulse emission ($GTP_P$) and a sustained change in emissions ($GTP_S$) of a given air

194    pollutant. The distinction between $GTP_P$ and $GTP_S$ avoids the overestimation of GWP for the short-

195    lived climate pollutants. Even for a uniform forcing, there will be differences of spatial patterns in the

196    temperature response. Regional Temperature-change Potential (RTP) (Shindell and Faluvegi, 2010)

197    was applied to analyze the temperature response on the regional scale, since both GWP and GTP

198    focused on the global scale. The GWP, GTP, and RTP were normalized to the corresponding effect of

199    $CO_2$ as the Absolute Global Warming Potential (AGWP), Absolute Global Temperature Change

200    Potential (AGTP), and Absolute Regional Temperature-change Potential (ARTP), respectively. AGWP

201    represented the absolute forms of radiative forcing. AGTP and ARTP represented the absolute forms

202    of temperature perturbation.

203       ARTPs is more suitable for this study to calculate the temperature response, considering that the

204    research object is BC with short lifetime and focus on regional impact of the BC emission reductions

205    on temperature changes in the Arctic. For SLCFs with atmospheric lifetimes much shorter than both

206    the time horizon of the ARTP and the response time of the climate system, the general expression for

207    the ARTP following a pulse emission of BC ($E$) in region $r$ which leads to a response in latitude band

208    $m$ is as follows (Fuglestvedt et al., 2010; Collins et al., 2013; Aamaas et al., 2017):

209    $\text{ARTP}_{r, m, s}(H) = \sum_l \frac{F_{l, r, s}}{E_{r, s}} \times \text{RCS}_{l, m} \times R_T(H)$                    (1)

210    $F_{l,r,s}$ (in W m$^{-2}$) is the radiative forcing in latitude band $l$ due to emission in region $r$ in season $s$ as a

211    function after the pulse emission $E_{r,s}$ (in Tg). Even though our estimates are based on seasonal

212    emissions, the temperature responses calculated are annual means. Shindell and Faluvegi (2009)

213    analyzed BC climate effect in four different latitudes: southern mid-high latitudes (90°S–28°S), tropics

214    (28°S–28°N), northern mid-latitudes (28°N–60°N), and the Arctic (60°N–90°N), which gives a better

215    estimate of the global temperature response as it accounts for varying efficacies with latitude. The

216    $RCS_{l,m}$ is a matrix of regional response coefficients based on the RTP concept (unitless; Collins et al.,

217    2013). As these response coefficients are normalized here, they contain no information on climate

218    sensitivity, only the relative regional responses in the different latitude bands. The global climate

219    sensitivity is included in the impulse response function R$_T$, which is a temporal temperature response

220    to an instantaneous unit pulse of RF (in K m$^2$ W$^{-1}$). This paper refers to the ARTP values in Aamaas et

221    al. (2017). Aamaas et al. (2017)  applies two refinements of the forcing-response coefficients for

222    radiative forcing occurring in the Arctic: one for the aerosol effects in the atmosphere (Shindell and

223    Faluvegi, 2010; Lund et al., 2014) and another for the effects due to BC on snow (Flanner, 2013). The

224    ARTP in this study estimated of the direct effect in the Arctic included both the direct radiative forcing

225    from outside the Arctic and within the Arctic, while the ARTP of the semi-direct effect in the Arctic

226    was due to the semi-direct radiative forcing from outside the Arctic. The contribution by radiative

227    forcing within the Arctic to Arctic temperature changes considered the vertical profile of BC

228    concentrations as both $F_{Arctic,r,s}$ and $RCS_{Arctic,Arctic}$ have a dependence on the height of the BC (Lund et

229    al., 2014; Lund et al., 2017). The total response in the Arctic was the sum of the contributions from

230    BC forcing outside of the Arctic and inside of the Arctic.

231    Regional temperature responses at time $t$ of an emission $E(t)$ can be calculated with these ARTP

232    values by a convolution (Aamaas et al., 2016). The temperature response is as follows:

233    $\Delta T_{r, m, s, t}(t) = \int_0^t E_{r, s, t}(t') \times \text{ARTP}_{r,m,s,t}(t-t') dt'$                    (2)

234    $\Delta T_{r,m,s,t}$ refers to the decrease of the Arctic or global surface temperature after 20, 100, or 500 years

235    to 20% BC emission reductions of six regions (namely EAS, EUR, MDE, NAM, RBU, and SAS) in

236    the framework of HTAP2 either during summer or winter.

**3. Results and Discussion**

**3.1 Model evaluation**

239    To evaluate the model performance from all six models, the monthly simulated surface BC

240    concentrations of the BASE case were compared with the observations at four monitoring sites in the

241    Arctic Circle in 2010. The locations of the four sites, including Alert (82.5°N, 62.3°W) in Canada,

242    Barrow (71.3°N, 156.6°W) in Alaska, Tiksi (71.59°N, 128.92°E) in Russia, and Zeppelin (78.9°N,

243    11.9°E) in Norway, are plotted in Figure S1 in the Supporting Information.

244        Metrics (Text S1) including correlative coefficient (COR), normalized mean bias (NMB),

245    normalized mean error (NME), mean bias (MB), and mean absolute error (MAE) were selected for

246    evaluating the model performance in this study (U.S. EPA, 2007) In addition to the evaluation for each

247    single model, the multi-model ensemble mean (calculated as the average of all participating models)

248    was also evaluated. The statistical results are listed in Table 3 and Table S1. A comparison between the

249    temporal variations of simulated and observed BC concentrations is shown in Figure S2.

250        The correlations of the simulated BC concentrations among different models were moderate to high

251    with CORs ranging from 0.33 to 0.98 (Table S1), suggesting the temporal variations of different

252    models were relatively consistent. Overall, CAMchem, GEOS-Chem, GOCART–v5, and OsloCTM3–

253    v2 underestimated the near-surface BC (Figure S2), which may be attributed to an underestimation of

254    BC emissions, e.g., gas flaring (Huang et al., 2014, 2015; Stohl et al., 2013) and shipping emissions

255    (Marelle et al., 2016). However, the simulated BC surface concentrations from CHASER_re1 and

256    CHASER_t106 were higher than those of the other four models and observations (Figure S2), which

257    were mainly due to their slow BC aging-rate in remote/polar regions (Sudo et al., 2015).

258        Table 3 shows the model performances at the four Arctic sites. Relatively good agreement between

259    the observation and models was found at Zeppelin, with CORs, NME, MB, and MAE of 0.59–0.83,

260    38.5%–142.6%, –13.5–15.0 ng m$^{-3}$, and 5.4–15.0 ng m$^{-3}$, respectively. On the contrary, the simulated

261    BC concentrations didn't agree so well with observations at the other three sites with even negative

262    COR values in some models (e.g., CAMchem, CHASER_re1, and CHASER_t106), which may be

263    explained by the uncertainties in emission inventory, the bias in the meteorological simulations, and

264    chemical mechanisms (Miao et al., 2017; Zhang et al., 2019). All models, except OsloCTM3,

265    overestimated the BC concentrations in Barrow in July (Figure S2), mainly due to the large

266    contributions of biomass burning from Siberia in the simulations caused by overestimations of

267    emissions and/or too little removal during transport (Sobhani et al., 2018). Although the single model

268    didn't reproduce the BC concentrations in the Arctic well, the consistency of the model ensemble mean

269    with the observation was improved to some extent. The NME and MAE of model ensemble mean was

270    closer to zero compared with the single model. Therefore, the multi-model ensemble mean was used

271    for further analysis.

272

273    **Table 3** Comparison between the simulated and observed monthly surface BC concentrations at Alert, Barrow, Tiksi,

274    and Zeppelin in 2010.

| Parameters | Sites | CAMchem | CHASER _re1 | CHASER _t106 | GEOS-Chem | GOCART –v5 | OsloCTM3 –v2 | Model ensemble mean |
|---|---|---|---|---|---|---|---|---|
| COR[a] | Alert | –0.24 | –0.22 | –0.15 | 0.35 | 0.20 | –0.24 | –0.10 |
| | Barrow | –0.28 | –0.08 | –0.06 | 0.06 | 0.00 | 0.01 | –0.06 |
| | Tiksi | –0.19 | 0.05 | –0.12 | 0.50 | 0.48 | 0.41 | 0.11 |
| | Zeppelin | 0.72 | 0.59 | 0.67 | 0.80 | 0.76 | 0.83 | 0.73 |
| NMB[b] | Alert | –86.75 | 115.06 | 100.97 | –57.81 | –34.31 | –92.38 | –9.21 |
| (%) | Barrow | –38.43 | 104.10 | 83.27 | –38.95 | –8.18 | –75.58 | 4.37 |
| | Tiksi | –82.03 | 10.31 | 12.90 | –69.76 | –67.34 | –84.82 | –46.79 |
| | Zeppelin | –79.93 | 142.64 | 120.44 | –45.57 | –9.81 | –75.98 | 8.63 |
| NME[c] | Alert | 86.75 | 151.30 | 147.94 | 66.37 | 70.77 | 92.38 | 74.69 |
| (%) | Barrow | 72.07 | 124.44 | 109.23 | 69.50 | 84.20 | 75.58 | 72.12 |
| | Tiksi | 82.03 | 64.55 | 72.45 | 70.16 | 68.82 | 84.82 | 60.81 |
| | Zeppelin | 79.93 | 142.64 | 120.44 | 45.57 | 38.59 | 75.98 | 42.06 |
| MB[d] | Alert | –29.03 | 11.08 | 8.74 | –21.41 | –16.07 | –30.16 | –12.81 |
| (ng m$^{-3}$) | Barrow | –22.13 | 15.35 | 10.77 | –19.10 | –11.12 | –30.40 | –9.44 |
| | Tiksi | –55.99 | –17.28 | –17.65 | –48.51 | –48.16 | –56.26 | –40.64 |
| | Zeppelin | –13.53 | 14.97 | 14.13 | –8.19 | –3.59 | –12.45 | –1.44 |
| MAE[e] | Alert | 29.03 | 31.05 | 31.55 | 22.85 | 22.23 | 30.16 | 23.56 |
| (ng m$^{-3}$) | Barrow | 29.01 | 28.91 | 27.82 | 26.71 | 30.30 | 30.40 | 25.22 |
| | Tiksi | 55.99 | 37.06 | 41.36 | 48.60 | 48.49 | 56.26 | 43.73 |
| | Zeppelin | 13.53 | 14.97 | 14.13 | 8.19 | 5.40 | 12.45 | 4.95 |

275    [a] Correlative coefficient. [b] Normalized mean bias. [c] Normalized mean error. [d] Mean bias. [e] Mean absolute error.

276    **3.2 Near-surface BC concentrations in the Arctic**

277    Before analyzing the responses of Arctic BC to emission reductions, it is necessary to understand the

278    spatial-temporal distribution of BC concentrations in the Arctic region. In this study, months from May

279    to October were defined as summer and November to April were defined as winter due to the special

280    geographical location of the Arctic (Aamaas et al., 2017).

281    The mean BC concentrations from the ensemble models near the Arctic surface (66–90°N) were

282    22.2 ng m$^{-3}$ during summer and 19.5 ng m$^{-3}$ during winter in 2010, respectively. Figure 2 shows that

283    the BC concentrations over the polar sea ice region in winter were much higher than that in summer.

284    The coverage of the polar dome expanded more southward in winter (Bozem et al., 2019; Law and

285    Stohl, 2007), allowing more BC from lower latitudinal regions to be transported into the Arctic.

286    Turbulent exchange and deposition were reduced during winter as the meteorological conditions in the

287    Arctic were stable and dry (Bradley et al., 1992; Bozem et al., 2019; Law and Stohl, 2007). In addition,

288    BC emissions in EAS, EUR, and RBU regions showed obvious monthly changes with higher emissions

289    from November to March as mentioned earlier (Section 2.1.1), leading to the relatively high BC

290    concentrations over the polar sea ice region in winter. Over the terrestrial areas within the Arctic Circle,

291    summer BC concentrations were higher than winter, especially in Siberia and Alaska, which were

292    attributed to intense BC emissions from biomass burning over these areas from Jun to Aug (Figure S3).

293



(a)                                          (b)
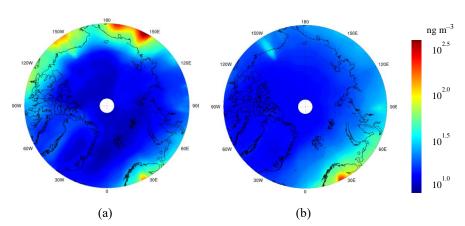
294    **Figure 2.** Spatial distribution of near-surface BC concentrations in **(a)** summer and **(b)** winter in the Arctic in 2010.
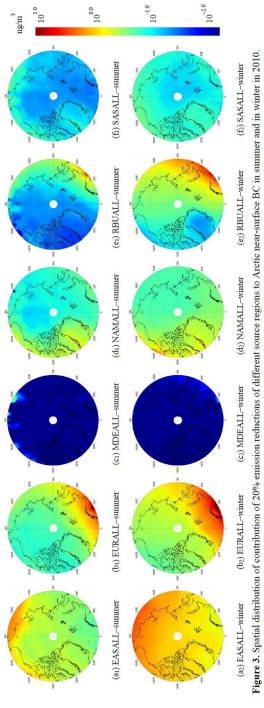
### 295   3.3 Response of Arctic BC to 20% emission reductions

### 296   3.3.1 Contributions of regional emission reductions to the Arctic near-surface BC

297   The response of the Arctic near-surface BC to 20% emission reductions from different source regions

298   was analyzed through emission perturbation simulations. Figure 3 shows the spatial distribution of the

299   referred response above in summer and winter of 2010 based on multi-model ensemble mean results.

300   The source region contributions to the surface BC concentrations exhibited significant seasonal

301   variability with higher values in winter. The BC emission reductions in EAS almost affected the whole

302   Arctic, especially in winter, indicating the significance of the intercontinental transport of BC. The

303   spatial distribution of the Arctic near-surface BC response to SAS emission reductions was similar to

304   that of EAS, but the extent was much weaker. The emission reductions from EUR, NAM, and RBU

305   mainly affected the local and nearby areas, which was generally consistent with the spatial pattern of

306   emissions (Figure 1). The contribution from MDE emission reductions was marginal.

307



**Figure 3.** Spatial distribution of contribution of 20% emission reductions of different source regions to Arctic near-surface BC in summer and in winter in 2010.

307

308

309    The monthly variations of the response of the Arctic near-surface BC concentrations to 20%

310    emission reductions from six source regions are presented in Figure 4. Results from the ensemble

311    simulations were averaged over the Arctic covering latitudinal areas from 66°N to the north pole. The

312    emission reductions from the total six source regions were 329.6 Gg in summer (May to October),

313    lower than that of 411.9 Gg in winter (November to April) (Table 1). Correspondingly, the contribution

314    from the six regions to the near-surface Arctic BC was 1.0–1.7 ng m$^{-3}$ in summer and 1.9–3.8 ng m$^{-3}$

315    in winter. Arctic sensitivities (Arctic concentration change per unit source region emission change) for

316    BC typically maximized from December to February for EUR and RBU and from March to May for

317    EAS and NAM (Shindell et al., 2008; AMAP, 2008). The enhanced sensitivity from December to May

318    resulted from faster transport and slower removal during winter as the meteorological conditions in

319    the Arctic were stable and dry (Law and Stohl, 2007). The results of deposition changes also proved

320    this result well (Figure S4). The wet deposition in summer was higher than that in winter, which was

321    3–10 times of dry depositions. Sharma et al. (2013) found that the Arctic region (north of 70°N) was

322    very dry during winter with an average daily precipitation rate between 0 and 1 mm day$^{-1}$. Precipitation

323    rates over some of the BC source regions such as Eurasia were at the same order of magnitude as the

324    Arctic. Less wet deposition and a shallow boundary layer resulted in higher BC concentrations near

325    the surface during winter. In the summertime, the Arctic region experienced 2 to 3 times higher

326    precipitation rates as well as wet depositions of BC relative to wintertime, thus resulting in lower

327    contributions to the near-surface BC concentrations.

328    The contribution of 20% BC emission reductions from EAS, EUR, MDE, NAM, RBU, and SAS to

329    the Arctic near-surface BC concentrations reached 0.88, 0.65, 0.01, 0.26, 0.29, and 0.11 ng m$^{-3}$,

330    respectively. Correspondingly, the reduced column BC loadings from the six regions above over the

331    Arctic was 8292.1, 2835.9, 28.8, 1774.6, 998.6, and 3381.1 ng m$^{-2}$, respectively.

332    The Arctic near-surface BC concentration response was found strongest to the 20% emission

333    reductions from EAS with the monthly contribution of 0.3–1.9 ng m$^{-3}$, accounting for 18.1%–51.4%

334    of the total reduced BC concentrations (Figure 4). On one hand, the BC emission reductions in EAS

335    were the largest among the six source regions (Table 1). On the other hand, BC emission reductions in

336    EAS can influence the Arctic lower troposphere via two pathways (Bozem et al., 2019; Stohl, 2006).

337    BC from northern regions of EAS can enter into the polar dome of the Arctic at low-level in winter, as

Atmospheric
Chemistry
and Physics
Discussions

Open Access

EGU

338   the air masses have cooled during transport. BC from eastern regions of EAS fast uplifted due to

339   convection and then followed by high altitude transport in northerly directions. Radiative cooling

340   eventually led to a slow descent into the polar dome area after air masses arrived in the high Arctic. It

341   occurred both in summer and winter. In addition to EAS, BC emission reduction from EUR also

342   showed significant impacts on the Arctic with the contribution of 0.3–1.2 ng m$^{-3}$, accounting for

343   20.1%–49.9% of the total reduced BC concentrations (Figure 4). Among the three regions in the Arctic

344   Circle (i.e. EUR, NAM, and RBU), EUR region had the largest BC emission reductions. Also, the

345   relatively short distance between EUR and the Arctic made EUR the second most important source

346   region to the Arctic. As for NAM and RBU, their 20% emission reductions induced moderate

347   reductions of the monthly Arctic near-surface BC concentrations by 0.1–0.4 and 0.1–0.7 ng m$^{-3}$,

348   respectively. The contribution of 20% emission reductions from SAS to the Arctic near-surface BC

349   concentrations was much lower of 0.1–0.2 ng m$^{-3}$ as a significant portion of BC originating from SAS

350   accumulated in the upper troposphere (Section 3.3.2). Compared to the five source regions discussed

351   above, the response of Arctic BC concentrations to emission reductions from MDE was negligible,

352   owing largely to the low emissions there and long distance from the Arctic.
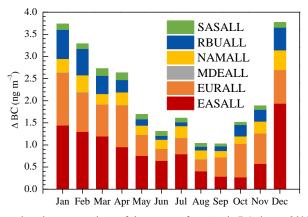
353



354   **Figure 4.** Monthly mean reduced concentrations of the near-surface Arctic BC due to 20% emission reductions of

355   six source regions in 2010.

356   **3.3.2 Contributions of regional emission reductions to the vertical BC profiles**

357       To assess the contributions from various source regions to the BC profiles based on the model

358   ensemble mean, the vertical stratification needed to be unified as most participating models had

359    different vertical settings. Since CHASER had a relatively low coarse vertical resolution of 32 layers,

360    the other models were unified to the same vertical stratification, as detailed in Table S2.

361        As shown in Figure 5, the contributions of regional emission reductions to BC exhibited strong

362    vertical gradients over the Arctic. In general, the BC profiles displayed a bimodal pattern in summer,

363    showing peaks at around 1.0–1.6 km a.s.l. (4th and 5th layer) and 8.0–9.7 km a.s.l. (13th – 15th layer).

364    While in winter, the BC profiles showed a unimodal pattern with peaks around 0.6–1.0 km a.s.l. (3rd

365    and 4th layer). Long-range transport of air pollutions may occur near the planetary boundary layer

366    (Eckhardt et al., 2003; Stohl et al., 2002). High contributions in the low layers (e.g., 3rd – 5th layers)

367    were consistent with the height of the planetary boundary layer in the Arctic (Zhang, et al., 2018;

368    Cheng, 2011).

369        It has been summarized that there were several major transport pathways for BC into the Arctic

370    troposphere (Stohl, 2006). i) BC transported rapidly at low-level, followed by uplifting at the Arctic

371    front when it was located far north. Significant deposition of BC in the Arctic occurred mostly north

372    of 70°N via this transport route. This transport route derived often from the high BC emission areas in

373    northern EUR but seldom from the NAM and RBU. That was mainly due to that the BC emissions

374    existed at high enough latitudes in EUR, which can be north of the polar front. However, the BC

375    emissions in NAM and RBU were concentrated south of the polar front (Figure 1), thus BC emitted

376    from these two regions can't be easily transported into the Arctic through this pathway. ii) Cold air

377    masses into the polar dome transported at low-level. This pathway derived mainly from EUR and high-

378    latitude areas of EAS during winter. The contribution of 20% emission reductions from EUR to the

379    Arctic BC concentrations peaked at around 1.0 km a.s.l. with the multi-model ensemble mean value

380    of 0.5 ng m$^{-3}$ in summer, while peaked at lower altitude of around 0.6 km a.s.l. with the value of 0.9

381    ng m$^{-3}$ in winter. iii) BC could also ascend south of the Arctic followed either by high–altitude transport

382    or by several cycles of upward and downward transport, and finally slowly descended into the polar

383    dome due to radiative cooling. This was the frequent transport route from source regions such as NAM,

384    RBU, and east EAS. The contribution from NAM and RBU to the Arctic BC peaked at about 1.6 km

385    a.s.l. (0.2 ng m$^{-3}$) and 1.0 km a.s.l. (0.2 ng m$^{-3}$) in summer, and peaked at about 0.6 km a.s.l. (0.4 ng

386    m$^{-3}$) and 0.4 km a.s.l. (0.5 ng m$^{-3}$) in winter. The contribution from EAS including pathways ii and iii,

387    to the Arctic BC peaked at about 1.6 km a.s.l. (0.7 ng m$^{-3}$) in summer and peaked at about 1.6 km a.s.l.

388    (1.7 ng m$^{-3}$) in winter. The contribution from MDE was negligible.

389    As shown in Figure 5, BC can also be transported into the upper troposphere of the Arctic. Air

390    masses preferably kept their potential temperature almost constant during transport as the atmospheric

391    circulation can be well described by adiabatic motions in the absence of diabatic processes related to

392    clouds, radiation, and turbulence. The potential temperature was low within the polar dome area, and

393    thus only air masses experienced diabatic cooling were able to enter the polar dome (Stohl, 2006). That

394    is to say, the air masses from SAS and low-latitude regions of EAS were not easy to penetrate the polar

395    dome but can be lifted and transported to the Arctic in the middle and upper troposphere along the

396    isentropes (AMAP, 2011; Barrie, 1986; Law and Stohl, 2007; Stohl, 2006). This agreed well with the

397    previous study of Koch and Hansen (2005). The contribution from SAS to the Arctic BC concentrations

398    peaked at about 9.7 km a.s.l. (0.4 ng m$^{-3}$) in both summer and winter. This was also consistent with

399    the vertical profiles of BC shown in Stjern et al. (2016). The polar dome boundary was variable in time

400    and space and was not zonally symmetric. The range of polar dome expanded southward to about 40°N

401    over Eurasia in winter as the temperature difference of different latitudes became smaller (Bozem et

402    al., 2019; Law and Stohl, 2007), resulting in the contribution of EAS to the Arctic BC concentrations

403    in upper troposphere only peak in summer at 13$^{th}$ layer (8.0 km a.s.l.) with the value of 0.5 ng m$^{-3}$.
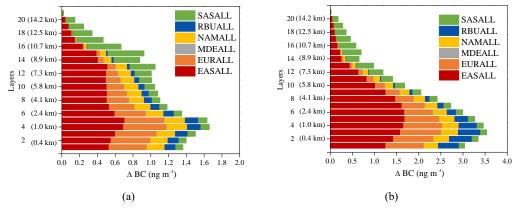
404



**Figure 5.** Contribution of 20% emission reductions of six source regions to BC concentrations in different vertical
layers **(a)** in summer and **(b)** in winter in the Arctic in 2010.

### 3.3.3 Contributions of emission reductions to BC in different latitudinal bands

408    To further analyze the response of the Arctic BC concentrations to emission reductions of six source

409   regions in HTAP2, the contribution of 20% emission reductions to BC concentrations at different

410   latitudes of the Arctic were calculated (Figures 6 and 7). In regard to the different horizontal resolution

411   of participating models, the Arctic region (66–90°N) was divided into eight latitudinal bands with a 3–

412   degree interval, which was based on the coarsest resolution of all models.

413       The response of the Arctic BC concentrations to emission reductions of six source regions became

414   weaker with the increase of the latitude due to the continuous loss of BC during transport (e.g., dry

415   and wet depositions) (Figure 6). The difference of contributions between two adjacent latitudinal bands

416   became smaller as closer to the north pole. The contributions of 20% emission reductions to the near-

417   surface Arctic BC concentrations were the highest between 66–69°N both in summer (2.3 ng m$^{-3}$) and

418   winter (4.6 ng m$^{-3}$), which were 1.3–2.6 times higher than the other latitudinal bands.

419       The contributions from EAS and EUR were higher than those from the other four regions in each

420   latitudinal band. In detail, the contributions from EUR (0.9 ng m$^{-3}$ in summer and 1.6 ng m$^{-3}$ in winter)

421   were higher than those from EAS (0.7 ng m$^{-3}$ in summer and 1.5 ng m$^{-3}$ in winter) in the latitudinal

422   band of 66–69°N as the near-surface BC concentrations there were more sensitive to the local emission

423   sources. In contrast, the contributions from EAS (0.4–0.6 ng m$^{-3}$ in summer and 1.1–1.3 ng m$^{-3}$ in

424   winter) were higher than those from EUR (0.2–0.6 ng m$^{-3}$ in summer and 0.5–1.0 ng m$^{-3}$ in winter) in

425   the other high latitudinal bands where long-range transport played the dominant role.
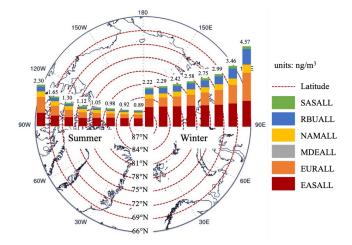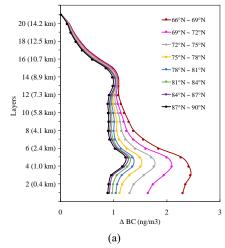
426



427

428   **Figure 6.** Contributions of 20% emission reductions of different regions to near-surface BC concentrations in each

429   latitudinal band of the Arctic. The results of summer and winter correspond to the left and right panel in the figure.

430

431    Figure 7 further depicts the response of the vertical Arctic BC concentrations to 20% emission

432    reductions. The contributions of eight latitudinal bands showed a typical bimodal pattern in summer

433    with peaks at 0.6–1.6 km a.s.l. ($3^{rd}$ – $5^{th}$ layer) and 8.0–8.9 km a.s.l. ($13^{th}$ and $14^{th}$ layer), while the

434    contribution displayed a single peak at the 0.4–1.0 km a.s.l. ($2^{nd}$ – $4^{th}$ layer) in winter. Similar to section

435    3.3.2, the peak value of the contribution at the low layer was due to the transport of EAS, EUR, NAM,

436    and RBU emission reductions to the Arctic through different pathways both in summer and winter. The

437    peak value in the high layer in summer was due to the transport of EAS and SAS. However, a high

438    contribution of 20% emission reductions to BC concentrations in SAS was found in the high layer,

439    while the contribution was low in other regions, leading to a single peak in winter. The statistical results

440    of SAS indicated that the contribution in vertical appeared one peak at the $15^{th}$ layer (9.7 km a.s.l.)

441    with a value of 0.40–0.44 ng $m^{-3}$ both in summer and winter (Figure S5).

442



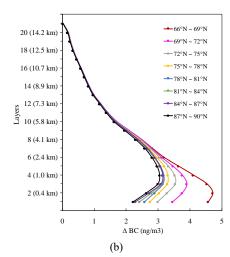(a)                                                                 (b)

443    **Figure 7.** Contributions of 20% emission reductions of all six source regions to the vertical BC concentrations of the
444    Arctic in different latitude bands varies with vertical layers in **(a)** summer and **(b)** winter in 2010.
445

446    As same as the whole Arctic region (section 3.3), the contributions of 20% emission reductions to

447    BC concentrations in eight latitude bands were higher in winter than in summer, whether near-surface

448    or in vertical. The total contribution of six source regions to BC concentrations in eight latitude bands

449    of the near-surface Arctic was 0.9–2.3 ng $m^{-3}$ in summer and 2.2–4.6 ng $m^{-3}$ in winter, respectively

450    (Figure 6). The peak of total contribution in vertical at the lower layer was 1.2–2.5 ng $m^{-3}$ in summer,

451    and 2.9–4.7 ng $m^{-3}$ in winter, respectively (Figure 7).

## 3.4 Benefit of BC emission reductions on the decrease of Arctic temperature

452

453 The impact of BC emission reductions on decreasing the Arctic (60–90°N) surface temperature was

454 assessed by using ARTP (See methods in Section 2.2). Aerosol effects, BC deposition on snow, and

455 BC semi-direct were considered in the calculation of ARTP (Aamaas et al., 2017). As shown in Figure

456 8, the response of Arctic temperature to emission reductions was the most significant at the time scale

457 of 10 years and then gradually decreased with the passage of time. For each source region, the Arctic

458 temperature response was significantly higher in winter than in summer as ARTP was seasonal

459 dependent with higher values in the warm seasons. Obviously, the Arctic benefited the most from

460 emission reduction from EAS with more than 300 and 660 μK decreases in summer and winter after

461 10 years, respectively. The influences of SAS and EUR emission reductions on the temperature

462 decrease in winter were similar, reaching about 10–320 μK and 14–370 μK after 10-100 years,

463 respectively. However, in summer, the influence of SAS on temperature decrease (8–230 μK) was

464 more than twice that of EUR (3–90 μK). Although the ARTP of EUR was higher than that of SAS, the

465 difference between emission reductions in the two regions was more obvious in summer (Table 1). The

466 temperature response to NAM in summer was similar to that from EUR, while this effect was weaker

467 than that from EUR in winter. This was mainly due to the smaller ARTP of NAM than EUR although

468 larger emission reductions were found from NAM. The temperature response to RBU was small due

469 to the low BC emission reductions even a high ARTP was associated with RBU. The minimum

470 temperature response was found from MDE due to the least emission reductions and small ARTP. In

471 spite of the higher Arctic temperature response to EAS than SAS in the target year of this study, a

472 number of studies have shown that BC emissions in South Asia were increasing in recent years (Sahu

473 et al., 2008; Paliwal et al., 2016; Sharma et al., 2019) while the emissions of East Asia were exhibiting

474 a downward trend especially from China (Chen et. al., 2016), thus it should be given more attention to

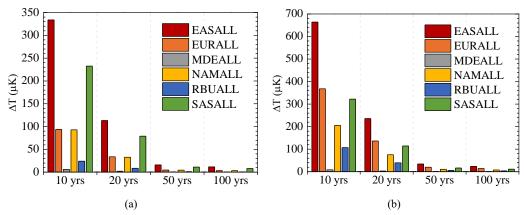475 the impact assessment of South Asia on the Arctic in the future.

476

**Figure 8.** Arctic temperature response to 20% regional BC emission reductions in **(a)** summer and **(b)** winter after 10, 20, 50, and 100 years.

In addition, the impacts of six source regions on the Arctic and global temperature were compared in this study. As shown in Figure 9, the Arctic and global temperature response to BC emission reductions from the six source regions ranged from about 27–780 μK and 10–290 μK in summer after 10, 20, 50, and 100 years, respectively, and they were about 61–1675 μK and 16–470 μK, respectively in winter. It can be seen that the difference of the temperature response between the Arctic and the globe was more obvious in winter. Overall, the Arctic temperature response was more sensitive to the whole globe in regard to the same emissions perturbation.
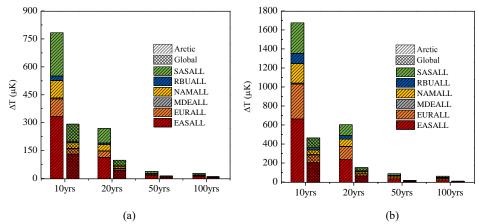


**Figure 9.** Global and Arctic temperature responses to 20% regional BC emission reductions in **(a)** summer and **(b)** winter after 10, 20, 50, and 100 years.

It should be noted the estimation of temperature response was subject to large uncertainties for the

492   following reasons. On the one hand, even though the HTAP2 emissions database were all constructed

493   by bottom-up methods, the different inventories and spatiotemporal distributions were constructed

494   with sub-regional (country, state, county or province level) activity data and emission factors, which

495   lead to inconsistencies at the borders between two adjacent inventories. The version 5 of Evaluating

496   the Climate and Air Quality Impacts of Short-Lived Pollutants (ECLIPSEv5, http://eclipse.nilu.no)

497   estimated a 2010 emission inventory, that serves also as a reference point for all projections (Janssens-

498   Maenhout et al., 2015). At the global level, a relatively good agreement was found with small relative

499   emission differences compared with the ECLIPSEv5 emission inventory for the aggregated sectors in

500   2010. However, larger differences of 29% between HTAP2 and ECLIPSEv5 emissions was present for

501   BC since ECLIPSEv5 relied on provincial statistics for China which resulted from higher coal

502   consumption than reported national statistics.

503       On the other hand, the time evolution of $R_T$, a parameter in the calculation of ARTP was also one

504   factor causing the uncertainty of temperature response calculation. This impulse response function was

505   only based on one coupled atmosphere-ocean climate model GISS-ER in this study, while Olivié and

506   Peters (2013) have found a spread in the GTP (20) value of BC of about −60 to +80% due to variability

507   of $R_T$ among various models. However, the uncertainty in $R_T$ was less relevant for the regional patterns.

508   Forcing-response coefficients didn't exist on a seasonal basis since emissions occurring during

509   Northern Hemisphere summer and winter season were differentiated (Aamaas et al, 2017). Hence, the

510   seasonal differences presented here in the ARTP values were not due to potential differences in the

511   response sensitivities, but due to differences in the RF. The temperature response will vary by species

512   and location, such as between land surface and ocean surface. These differences are not accounted for

513   in this study, but the increased efficacy in the RCS matrix towards the NH can be partly attributed to a

514   larger land area fraction in the NH (Shindell et al., 2015). Besides, recent studies have found that the

515   positive radiation budget of BC has been largely compensated by rapid atmospheric adjustment, this

516   means that the responses of surface temperatures to BC could be weaker than expected (Stjern et al.,

517   2017; Takemura and Suzuki, 2019).

518       Although the HTAP2 emissions database contain uncertainties and ARTP calculations are

519   simplifications, these emission metrics are useful, simple, and quick approximations for calculating

520   the temperature response in the different latitude bands for emissions of BC.

## 4. Conclusions

521

522    The CAMchem, CHASER_re1, CHASER_t106, GEOS-Chem, GOCART, and Oslo CTM3 in

523    HTAP2 experiment were used in this study to estimate the responses of Arctic BC to multi-region

524    emission reductions in 2010. Six regions (e.g., EAS, EUR, MDE, RBU, NAM, and SAS) were selected

525    as the source regions and the Arctic was the receptor region. HTAP2 set up the base scenario with all

526    BC emissions, and also simulated BC concentrations with 20% reduction of anthropogenic emissions.

527    The AGPT was further used to calculate the benefit of BC emission reductions on the decrease of

528    Arctic temperature.

529    The statistical results of 20% BC emission reductions showed that emission reductions in EAS were

530    the largest with the values of 355.6 Gg yr$^{-1}$, followed by SAS (232.5 Gg yr$^{-1}$), EUR (65.3 Gg yr$^{-1}$),

531    NAM (62.2 Gg yr$^{-1}$), RBU (18.6 Gg yr$^{-1}$), and MDE (5.3 Gg yr$^{-1}$). The BC emission reductions in the

532    EAS, EUR, and RBU were higher from November to March.

533    The temporal variations of simulations from different models were relatively consistent as the

534    correlations of the simulated BC concentrations among different models ranged from 0.33 to 0.98.

535    However, the simulated BC concentrations didn't agree so well with observations at monitoring sites

536    except Zeppelin. The consistency of the model ensemble mean value with the observation was

537    significantly improved and the results were acceptable to use for further analysis.

538    The contribution of 20% BC emission reductions from EAS, EUR, MDE, NAM, RBU, and SAS to

539    the Arctic near-surface BC concentrations reached 0.88, 0.65, 0.01, 0.26, 0.29, and 0.11 ng m$^{-3}$,

540    respectively. Correspondingly, the reduced column BC loadings from the six regions above over the

541    Arctic was 8292.1, 2835.9, 28.8, 1774.6, 998.6, and 3381.1 ng m$^{-2}$, respectively.

542    BC emission reduction from EAS and EUR showed significant impacts on the near-surface Arctic

543    with the contribution of 0.3–1.9 ng m$^{-3}$ and 0.3–1.2 ng m$^{-3}$, accounting for 18.1%–51.4% and 20.1%–

544    49.9% of the total reduced BC concentrations, respectively. The BC profiles displayed a bimodal

545    pattern in summer with peaks at around 1.0–1.6 km a.s.l. (4$^{th}$ and 5$^{th}$ layer) and 8.0–9.7 km a.s.l. (13$^{th}$

546    – 15$^{th}$ layer). While the BC profiles showed a unimodal pattern with peaks around 0.6–1.0 km a.s.l.

547    (3$^{rd}$ and 4$^{th}$ layer) in winter.

548    The response of Arctic BC to emission reductions from source regions in winter was higher than

549    that in summer. The contributions of 20% emission reductions to the near-surface Arctic BC

550    concentrations were the highest between 66–69°N both in summer (2.3 ng m$^{-3}$) and winter (4.6 ng m$^{-}$

551    $^3$), and became weaker with the increase of the latitude.

552       The response of Arctic temperature to BC emission reductions was the most significant at the time

553    scale of 10 years and then gradually decreased with the passage of time. The Arctic had benefited the

554    most from emission reduction in EAS with more than 300 and 660 μK decreases in summer and winter

555    after 10 years, respectively. The Arctic temperature response was more sensitive to the whole globe in

556    regard of the same emissions perturbation. The estimation of temperature response was subject to large

557    uncertainties due to the uncertainties in the calculation of ARTP and emissions of BC in source regions.

558       Overall, this study provided insights on the source regions and seasonal contributions of Arctic BC

559    from the most recent international ensemble modeling efforts. The discrepancy between model results

560    and observations and the spread among different HTAP models may be attributed to various factors

561    such as emissions in the remote Arctic, physical parameterizations, and convection and deposition

562    processes. This would subsequently result in large uncertainties of the climatic effects of air pollutants.

563    More observation sites on the typical transport pathways from sources regions to the Arctic should be

564    planned to improve the model capability of simulating the transport behavior of black carbon.

565    **Data availability**

566    All data used in this study can be obtained through the AeroCom servers and web interfaces,

567    accessible at http://aerocom.met.no.

568

569    **Author contributions**

570    KH and JSF designed this study. ML, KS, DH, TK, MC, and ST performed modeling. NZ analyzed

571    data and wrote the paper. All have commented on and reviewed the paper.

572

573 **Competing interests.**

574 The authors declare that they have no conflict of interest.
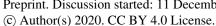
575

576 **Acknowledgements**

580

## *References*

Aamaas, B., Berntsen, T. K., Fuglestvedt, J. S., Shine, K. P., and Bellouin, N.: Regional emission metrics for short–lived climate forcers from multiple models, Atmos. Chem. Phys., 16, 7451– 7468, https://doi.org/10.5194/acp–16–7451–2016, 2016.

Aamaas, B., Berntsen, T. K., Fuglestvedt, J. S., Shine, K. P., and Collins, W. J.: Regional temperature change potentials for short-lived climate forcers based on radiative forcing from multiple models, Atmos. Chem. Phys., 17, 10795-10809, 10.5194/acp-17-10795-2017, 2017.

AMAP: Black carbon and ozone as Arctic climate forcers. Arctic Monitoring and Assessment Programme (AMAP), Oslo, Norway. vii + 116 pp, 2015.

AMAP: Snow, Water, Ice and Permafrost in the Arctic (SWIPA) 2017. Arctic Monitoring and Assessment Programme (AMAP), Oslo, Norway. xiv + 269 pp. ISBN 978–82–7971–101–8, 2017.

AMAP: The Impact of Black Carbon on Arctic Climate. By: Quinn, P. K., Stohl, A., Arneth, A., Berntsen, T., Burkhart, J. F., Christensen, J., Flanner, M., Kupiainen, K., Lihavainen, H., Shepherd, M., Shevchenko, V., Skov, H., and Vestreng., V., Arctic Monitoring and Assessment Programme (AMAP), Oslo. 72 pp, 2011.

AMAP: The Impact of Short–Lived Pollutants on Arctic Climate. By: Quinn, P. K., Bates, T. S., Baum, E., Bond, T., Burkhart, J. F., Fiore, A. M., Flanner, M. G., Garrett, T., Koch, D., Mcconnell, J. R., Shindell, D., and Stohl, A., Arctic Monitoring and Assessment Programme (AMAP), Oslo, Norway, 2008.

Barrie, L. A.: Arctic air pollution: an overview of current knowl- edge, Atmos. Environ., 20, 643–663, 1986.

Bond, T. C., Doherty, S. J., Fahey, D. W., Forster, P. M., Berntsen, T., DeAngelo, B. J., Flanner, M. G., Ghan, S., Kärcher, B., Koch, D., Kinne, S., Kondo, Y., Quinn, P. K., Sarofim, M. C., Schultz, M. G., Schulz, M., Venkataraman, C., Zhang, H., Zhang, S., Bellouin, N., Guttikunda, S. K., Hopke, P. K., Jacobson, M. Z., Kaiser, J. W., Klimont, Z., Lohmann, U., Schwarz, J. P., Shindell, D., Storelvmo, T., Warren, S. G., and Zender, C. S.: Bounding the role of black carbon in the climate system: A scientific assessment, J. Geophys. Res.–Atmos., 118, 5380–5552, https://doi.org/10.1002/jgrd.50171, 2013.

Bozem, H., Hoor, P., Kunkel, D., Köllner, F., Schneider, J., Herber, A., Schulz, H., Leaitch, W. R., Aliabadi, A. A., Willis, M. D., Burkart, J., and Abbatt, J. P. D.: Characterization of transport regimes and the polar dome during Arctic spring and summer using in situ aircraft measurements, Atmos. Chem. Phys., 19, 15049-15071, 10.5194/acp-19-15049-2019, 2019.

Bradley, R. S., Keimig, F. T., and Diaz, H. F.: Climatology of surface-based inversions in the North American Arctic, J. Geophys. Res., 97, 15 699, https://doi.org/10.1029/92JD01451, 1992.

Chen, D. S., Zhao, Y. H., Nelson, P., Li, Y., Wang, X. T., Zhou, Y., Lang, J. L., and Guo, X. R.: Estimating ship emissions based on AIS data for port of Tianjin, China. Atmos. Environ. 145: 10–18. http://dx.doi.org/10.1016/j.atmosenv.2016.

Cheng, G.: Analysis of observational data of atmospheric boundary layer characteristics in the Arctic (in Chinese), Nanjing University of information engineering. 2011.

Chin, M., Rood, R. B., Lin, S.–J., Müller, J.–F., and Thompson, A. M.: Atmospheric sulfur cycle simulated in the global model GOCART: Model description and global properties, J. Geophys. Res.–Atmos., 105, 24671–24687, doi:10.1029/2000JD900384, 2000.

Clarke, A. D. and Noone, K. J.: Soot in the Arctic snowpack: a cause for perturbations in radiative transfer, Atmos. Environ., 19, 2045–2053, https://doi.org/10.1016/0004-6981(85)90113-1, 1985.

Collins, W. J., Fry, M. M., Yu, H., Fuglestvedt, J. S., Shindell, D. T., and West, J. J.: Global and regional temperature-

622     change potentials for near-term climate forcers, Atmos. Chem. Phys., 13, 2471-2485, 10.5194/acp-13-2471-
623     2013, 2013.

624 Eckhardt, S., Stohl, A., Beirle, S., Spichtinger, N., James, P., Forster, C., Junker, C., Wagner, T., Platt, U., and Jennings,
625     S. G.: The North Atlantic Oscillation controls air pollution transport to the Arctic, Atmos. Chem. Phys., 3, 1769–
626     1778, https://doi.org/10.5194/acp–3–1769–2003, 2003.

627 Flanner, M. G.: Arctic climate sensitivity to local black carbon, J. Geophys. Res.-Atmos., 118, 1840–1851,
628     https://doi.org/10.1002/jgrd.50176, 2013.

629 Fuglestvedt, J. S., Shine, K. P., Berntsen, T., Cook, J., Lee, D. S., Stenke, A., Skeie, R. B., Velders, G. J. M., and
630     Waitz, I. A.: Transport impacts on atmosphere and climate: metrics, Atmos. Environ., 44, 4648–4677,
631     https://doi:10.1016/j.atmosenv.2009.04.044, 2010.

632 Galmarini, S., Koffi, B., Solazzo, E., Keating, T., Hogrefe, C., Schulz, M., Benedictow, A., Griesfeller, J. J., Janssens-
633     Maenhout, G., Carmichael, G., Fu, J., and Dentener, F.: Technical note: Coordination and harmonization of the
634     multi-scale, multi-model activities HTAP2, AQMEII3, and MICS-Asia3: simulations, emission inventories,
635     boundary conditions, and model output formats, Atmos. Chem. Phys., 17, 1543–1555, 2017.

636 Garrett, T. J. and Zhao, C.: Increased Arctic cloud longwave emissivity associated with pollution from mid-latitudes,
637     Nature, 440, 787–789, 2006.Hansen, J. and Nazarenko, L.: Soot climate forcing via snow and ice albedos, P.
638     Natl Acad. Sci. USA, 101, 423–428, https://doi.org/10.1073/pnas.2237157100, 2004.

639 Henze, D. K., Hakami, A., and Seinfeld, J. H.: Development of the adjoint of GEOS–Chem, Atmos. Chem. Phys., 7,
640     2413–2433, doi:10.5194/acp–7–2413–2007, 2007.

641 Hogrefe, C., Liu, P., Pouliot, G., Mathur, R., Roselle, S., Flemming, J., Lin, M., and Park, R. J.: Impacts of different
642     characterizations of large-scale background on simulated regional-scale ozone over the continental United States,
643     Atmos. Chem. Phys., 18, 3839–3864, 2018.

644 Huang, K., Fu, J. S., Hodson, E. L., Dong, X., Cresko, J., Prikhodko, V. Y., Storey, J. M., and Cheng, M.-D.:
645     Identification of missing anthropogenic emission sources in Russia: Implication for modeling Arctic haze,
646     Aerosol Air Qual. Res., 14, 1799–1811, 2014.

647 Huang, K., Fu, J. S., Prikhodko, V. Y., Storey, J. M., Ro- manov, A., Hodson, E. L., Cresko, J., Morozova, I., Ig-
648     natieva, Y., and Cabaniss, J.: Russian anthropogenic black carbon: Emission reconstruction and Arctic black
649     carbon simulation, J. Geophys. Res.-Atmos., 120, 11306–11333, https://doi.org/10.1002/2015JD023358, 2015.

650 IPCC: Climate Change: The Intergovernmental Panel on Climate Change Scientific Assessment. The
651     Intergovernmental Panel on Climate Change (IPCC), Cambridge University Press, Cambridge, UK, 1990.

652 IPCC: Climate Change 2001: The Scientific Basis. Intergovernmental Panel on Climate Change. The
653     Intergovernmental Panel on Climate Change (IPCC), Cambridge University Press, Cambridge, UK, 2001.

654 Janssens-Maenhout, G., Crippa, M., Guizzardi, D., Dentener, F., Muntean, M., Pouliot, G., Keating, T., Zhang, Q.,
655     Kurokawa, J., Wankmüller, R., Denier van der Gon, H., Kuenen, J. J. P., Klimont, Z., Frost, G., Darras, S., Koffi,
656     B., and Li, M.: HTAP_v2.2: a mosaic of regional and global emission grid maps for 2008 and 2010 to study
657     hemispheric transport of air pollution, Atmos. Chem. Phys., 15, 11411-11432, 10.5194/acp-15-11411-2015,
658     2015.

659 Jonson, J. E., Schulz, M., Emmons, L., Flemming, J., Henze, D., Sudo, K., Tronstad Lund, M., Lin, M., Benedictow,
660     A., Koffi, B., Dentener, F., Keating, T., Kivi, R., and Davila, Y.: The effects of intercontinental emission sources
661     on European air pollution levels, Atmos. Chem. Phys., 18, 13655–13672, 2018.

662 Koch, D. and Hansen, J.: Distant origins of Arctic black carbon: A Goddard Institute for Space Studies ModelE
663     experiment, J. Geophys. Res.–Atmos., 110, D04204, https://doi.org/10.1029/2004JD005296, 2005.

664 Lamarque, J. F., Emmons, L. K., Hess, P. G., Kinnison, D. E., Tilmes, S., Vitt, F., Heald, C. L., Holland, E. A.,

665    Lauritzen, P. H., Neu, J., Orlando, J. J., Rasch, P. J., and Tyndall, G. K.: CAM-chem: description and evaluation
666        of interactive atmospheric chemistry in the Community Earth System Model, Geosci. Model Dev., 5, 369-411,
667        10.5194/gmd-5-369-2012, 2012.
668    Law, K. S. and Stohl, A.: Arctic air pollution: origins and impacts, Science, 315, 1537–1540,
669        https://doi.org/10.1126/science.1137695, 2007.
670    Liang, C.-K., West, J. J., Silva, R. A., Bian, H., Chin, M., Davila, Y., Dentener, F. J., Emmons, L., Flemming, J.,
671        Folberth, G., Henze, D., Im, U., Jonson, J. E., Keating, T. J., Kucsera, T., Lenzen, A., Lin, M., Lund, M. T., Pan,
672        X., Park, R. J., Pierce, R. B., Sekiya, T., Sudo, K., and Takemura, T.: HTAP2 multi-model estimates of premature
673        human mortality due to intercontinental transport of air pollution and emission sectors, Atmos. Chem. Phys., 18,
674        10497–10520, 2018.
675    Lund, M. T., Berntsen, T. K., Heyes, C., Klimont, Z., and Samset, B. H.: Global and regional climate impacts of black
676        carbon and co-emitted species from the on-road diesel sector, Atmos. Envi- ron., 98, 50–58,
677        https://doi.org/10.1016/j.atmosenv.2014.08.033, 2014.
678    Lund, M. T., Aamaas, B., Berntsen, T., Bock, L., Burkhardt, U., Fuglestvedt, J. S., and Shine, K. P.: Emission metrics
679        for    quantifying    regional    climate    impacts    of    aviation,    Earth    Syst.    Dynam.,    8,    547–563,
680        https://doi.org/10.5194/esd-8-547-2017, 2017.
681    Lund, M. T., Myhre, G., Haslerud, A. S., Skeie, R. B., Griesfeller, J., Platt, S. M., Kumar, R., Myhre, C. L., and
682        Schulz, M.: Concentrations and radiative forcing of anthropogenic aerosols from 1750 to 2014 simulated with
683        the    Oslo    CTM3    and    CEDS    emission    inventory,    Geosci.    Model    Dev.,    11,    4909–4931,
684        https://doi.org/10.5194/gmd-11-4909-2018, 2018.
685    Marelle, L., Thomas, J. L., Raut, J.-C., Law, K. S., Jalkanen, J.- P., Johansson, L., Roiger, A., Schlager, H., Kim, J.,
686        Reiter, A., and Weinzierl, B.: Air quality and radiative impacts of Arctic shipping emissions in the summertime
687        in    northern    Norway:    from    the    local    to    the    regional    scale,    Atmos.    Chem.    Phys.,    16,    2359– 2379,
688        https://doi.org/10.5194/acp-16-2359-2016, 2016.
689    Miao, Y. C., Guo, J. P., Liu, S. H., Liu, H., Zhang, G., Yan, Y., He, J.: Relay transport of aerosols to Beijing–Tianjin–
690        Hebei    region    by    multiscale    atmospheric    circulations,    Atmos.    Environ.,    165,    35–45,
691        https://doi.org/10.1016/j.atmosenv.2017.06.032, 2017.
692    Myhre, G., Shindell, D., Breon, F.–M., Collins, W., Fuglestvedt, J., Huang, J., Koch, D., Lamarque, J.–F., Lee, D.,
693        Mendoza, B., Nakajima, T., Robock, A., Stephens, G., Takemura, T., and Zhang, H.: Anthropogenic and Natural
694        Radiative Forcing, in: Climate Change 2013: The Physical Science Basis. Contribution of Working Group I to
695        the Fifth Assessment Report of the Inter– governmental Panel on Climate Change, edited by: Stocker, T. F., Qin,
696        D., Plattner, G.–K., Tignor, M., Allen, S. K., Boschung, J., Nauels, A., Xia, Y., Bex, V., and Midgley, P. M.,
697        Cambridge Uni– versity Press, Cambridge, UK and New York, NY, USA, 2013.
698    Olivié, D. J. L. and Peters, G. P.: Variation in emission metrics due to variation in $CO_2$ and temperature impulse
699        response functions, Earth Syst. Dynam., 4, 267–286, https://doi.org/10.5194/esd-4- 267-2013, 2013.
700    Paliwal, U., Sharma, M., and Burkhart, J. F.: Monthly and spatially resolved black carbon emission inventory of India:
701        uncertainty analysis, Atmos. Chem. Phys., 16, 12457-12476, 10.5194/acp-16-12457-2016, 2016.
702    Sahu, S. K., Beig, G., and Sharma, C.: Decadal growth of black carbon emissions in India, Geophysical Research
703        Letters, 35, 10.1029/2007gl032333, 2008.
704    Samset, B. H., Myhre, G., Schulz, M., Balkanski, Y., Bauer, S., Berntsen, T. K., Bian, H., Bellouin, N., Diehl, T.,
705        Easter, R. C., Ghan, S. J., Iversen, T., Kinne, S., Kirkevåg, A., Lamarque, J. F., Lin, G., Liu, X., Penner, J. E.,
706        Seland, Ø., Skeie, R. B., Stier, P., Takemura, T., Tsigaridis, K., and Zhang, K.: Black carbon vertical profiles
707        strongly affect its radiative forcing uncertainty, Atmos. Chem. Phys., 13, 2423-2434, 10.5194/acp-13-2423-2013,

708     2013.

709     Sand, M., Berntsen, T. K., von Salzen, K., Flanner, M. G., Langner, J., and Victor, D. G.: Response of Arctic
710          temperature to changes in emissions of short–lived climate forcers, Nature Clim. Change, 6, 286–289,
711          10.1038/nclimate2880, 2016.

712     Sekiya, T., Miyazaki, K., Ogochi, K., Sudo, K., and Takigawa, M.: Global high-resolution simulations of tropospheric
713          nitrogen dioxide using CHASER V4.0, Geosci. Model Dev., 11, 959-988, 10.5194/gmd-11-959-2018, 2018.

714     Sharma, S., Ishizawa, M., Chan, D., Lavoué, D., Andrews, E., Eleftheriadis, K., and Maksyutov, S.: 16-year
715          simulation of Arctic black carbon: Transport, source contribution, and sensitivity analysis on deposition, Journal
716          of Geophysical Research: Atmospheres, 118, 943-964, 10.1029/2012jd017774, 2013.

717     Sharma, G., Sinha, B., Pallavi, Hakkim, H., Chandra, B. P., Kumar, A., and Sinha, V.: Gridded Emissions of CO, NO
718          x, SO2, CO2, NH3, HCl, CH4, PM2.5, PM10, BC, and NMVOC from Open Municipal Waste Burning in India,
719          Environ Sci Technol, 53, 4765-4774, 10.1021/acs.est.8b07076, 2019.

720     Shine, K. P., Fuglestvedt, J. S., Hailemariam, K., and Stuber, N.: Alternatives to the Global Warming Potential for
721          Comparing Climate Impacts of Emissions of Greenhouse Gases, Climatic Change, 68, 281–302,
722          10.1007/s10584–005–1146–9, 2005

723     Shindell, D. and Faluvegi, G.: Climate response to regional radiative forcing during the 20th century, Nat. Geosci.,
724          2, 294–300, 2009.

725     Shindell, D. and Faluvegi, G.: The net climate impact of coal–fired power plant emissions, Atmos. Chem. Phys., 10,
726          3247–3260, https://doi.org/10.5194/acp–10–3247–2010, 2010.

727     Shindell D., Kuylenstierna J.C.I., Vignati E., van Dingenen R., Amann M., Klimont Z., Anenberg S.C., Muller N.,
728          JanssensMaenhaut G., Raes F., Schwartz J., Faluvegi G., Pozzoli L., Kupiainen K., Höglund–Isaksson L.,
729          Emberson L., Streets D., Ramanathan V., Hicks K., Kim Oanh N.T., Milly G., Williams M., Demkine W., Fowler
730          D.: Simultaneously Mitigating Near–Term Climate Change and Improving Human Health and Food Security.
731          Science, Vol. 335, 183–189, 2012.

732     Shindell, D. T., Chin, M., Dentener, F., Doherty, R. M., Faluvegi, G., Fiore, A. M., Hess, P., Koch, D. M., MacKenzie,
733          I. A., Sanderson, M. G., Schultz, M. G., Schulz, M., Stevenson, D. S., Teich, H., Textor, C., Wild, O., Bergmann,
734          D. J., Bey, I., Bian, H., Cuvelier, C., Duncan, B. N., Folberth, G., Horowitz, L. W., Jonson, J., Kaminski, J. W.,
735          Marmer, E., Park, R., Pringle, K. J., Schroeder, S., Szopa, S., Takemura, T., Zeng, G., Keating, T. J., Zuber, A.:
736          A multi–model assessment of pollution transport to the Arctic, Atmos. Chem. Phys. Discuss., 2008.

737     Shindell, D. T., Faluvegi, G., Rotstayn, L., and Milly, G.: Spatial patterns of radiative forcing and surface temperature
738          response, J. Geophys. Res.-Atmos., 120, 5385–5403, https://doi.org/10.1002/2014JD022752, 2015.

739     Shindell, D. T., Lamarque, J.–F., Schulz, M., Flanner, M., Jiao, C., Chin, M., Young, P. J., Lee, Y. H., Rotstayn, L.,
740          Mahowald, N., Milly, G., Faluvegi, G., Balkanski, Y., Collins, W. J., Conley, A. J., Dalsoren, S., Easter, R., Ghan,
741          S., Horowitz, L., Liu, X., Myhre, G., Nagashima, T., Naik, V., Rumbold, S. T., Skeie, R., Sudo, K., Szopa, S.,
742          Takemura, T., Voulgarakis, A., Yoon, J.–H., and Lo, F.: Radiative forcing in the ACCMIP historical and future
743          climate simulations, Atmos. Chem. Phys., 13, 2939–2974, 2013.

744     Shindell, D. T., Voulgarakis, A., Faluvegi, G., and Milly, G.: Precipitation response to regional radiative forcing,
745          Atmos. Chem. Phys., 12, 6969–6982, doi:10.5194/acp–12–6969–2012, 2012.

746     Smith, S.J. and Mizrahi, A.: Near–term climate mitigation by short–lived forcers. PNAS 14202–14206, doi:
747          10.1073/pnas.1308470110, 2013.

748     Sobhani, N., Kulkarni, S., Carmichael, G. R.: Source sector and region contributions to black carbon and $PM_{2.5}$ in
749          the Arctic. Atmos. Chem. Phys., 18, 18123–18148, 2018.

750     Stjern, C. W., Samset, B. H., Myhre, G., Bian, H., Chin, M., Davila, Y., Dentener, F., Emmons, L., Flemming, J.,

751    Haslerud, A. S., Henze, D., Jonson, J. E., Kucsera, T., Lund, M. T., Schulz, M., Sudo, K., Takemura, T., and
752        Tilmes, S.: Global and regional radiative forcing from 20 % reductions in BC, OC and SO4 – an HTAP2 multi-
753        model study, Atmos. Chem. Phys., 16, 13579–13599, https://doi.org/10.5194/acp-16-13579-2016, 2016.

754    Stjern, C. W. et al. Rapid adjustments cause weak surface temperature response to increased black carbon
755        concentrations. Geophys. Res. 122, 11462–11481, 2017.

756    Stohl, A.: Characteristics of atmospheric transport into the Arctic troposphere, J. Geophys. Res., 111, D11306,
757        https://doi.org/10.1029/2005JD006888, 2006.

758    Stohl A., Aamaas B., Amann M., Baker L. H., Bellouin N., Berntsen T. K., Boucher O., Cherian R., Collins W.,
759        Daskalakis N., Dusinska M., Eckhardt S., Fuglestvedt J. S., Harju M., Heyes C., Hodnebrog Ø., Hao J., Im U.,
760        Kanakidou M., Klimont Z., Kupiainen K., Law K. S., Lund M. T., Maas R., MacIntosh C. R., Myhre G.,
761        Myriokefalitakis S., Olivié D., Quaas J., Quennehen B., Raut J.–C., Rumbold S. T., Samset B. H., Schulz M.,
762        Seland Ø., Shine K. P., Skeie R. B., Wang S., Yttri K. E., and Zhu T.: Evaluating the climate and air quality
763        impacts of short–lived pollutants. Atmos. Chem. Phys., 15, 10529 – 10566, 2015.

764    Stohl, A., Eckhardt, S., Forster, C., James, P., and Spichtinger, N.: On the pathways and timescales of intercontinental
765        air pollution transport, J. Geophys. Res.–Atmos., 107, ACH 6–1–ACH 6–17,
766        https://doi.org/10.1029/2001JD001396, 2002.

767    Stohl, A., Klimont, Z., Eckhardt, S., Kupiainen, K., Shevchenko, V. P., Kopeikin, V. M., and Novigatsky, A. N.: Black
768        carbon in the Arctic: the underestimated role of gas flaring and residential combustion emissions, Atmos. Chem.
769        Phys., 13, 8

770    Sudo, K., Sekiya, T., Nagashima, T.: CHASER/MIROC-ESM in HTAP2 status reports, HTAP2 Global and Regional
771        Model Evaluation Workshop, Nagoya University, JAMSTEC, NIES, 2015.

772    Sudo, K., Takahashi, M., Kurokawa, J.–I., and Akimoto, H.: CHASER: A global chemical model of the troposphere
773        1. Model description, J. Geophys. Res.–Atmos., 107, ACH 7–1–ACH 7–20, doi:10.1029/2001JD001113, 2002.

774    Søvde, O. A., Prather, M. J., Isaksen, I. S. A., Berntsen, T. K., Stordal, F., Zhu, X., Holmes, C. D., and Hsu, J.: The
775        chemical transport model Oslo CTM3, Geosci. Model Dev., 5, 1441–1469, doi:10.5194/gmd–5–1441–2012,
776        2012.

777    Takemura, T., and Suzuki, K.: Weak global warming mitigation by reducing black carbon emissions, Scientific
778        Reports, 9, 10.1038/s41598-019-41181-6, 2019.

779    Tan, J., Fu, J. S., Dentener, F., Sun, J., Emmons, L., Tilmes, S., Sudo, K., Flemming, J., Jonson, J. E., Gravel, S.,
780        Bian, H., Davila, Y., Henze, D. K., Lund, M. T., Kucsera, T., Takemura, T., and Keating, T.: Multi-model study
781        of HTAP II on sulfur and nitrogen deposition, Atmos. Chem. Phys., 18, 6847–6866, 2018a.

782    Tan, J., Fu, J. S., Dentener, F., Sun, J., Emmons, L., Tilmes, S., Flemming, J., Takemura, T., Bian, H., Zhu, Q., Yang,
783        C.-E., and Keating, T.: Source contributions to sulfur and nitrogen deposition – an HTAP II multi-model study
784        on hemispheric transport, Atmos. Chem. Phys., 18, 12223–12240, 2018b.

785    Teng, H., Washington, W. M., Branstator, G., Meehl, G. A., and Lamarque, J.–F.: Potential impacts of Asian carbon
786        aerosols on future US warming, Geophys. Res. Lett., 39, L11703, doi:10.1029/2012GL051723, 2012.

787    Tilmes, S., Lamarque, J.–F., Emmons, L. K., Kinnison, D. E., Marsh, D., Garcia, R. R., Smith, A. K., Neely, R. R.,
788        Conley, A., Vitt, F., Val Martin, M., Tanimoto, H., Simpson, I., Blake, D. R., and Blake, N.: Representation of
789        the Community Earth System Model (CESM1) CAM4–chem within the Chemistry– Climate Model Initiative
790        (CCMI), Geosci. Model Dev., 9, 1853– 1890, doi:10.5194/gmd–9–1853–2016, 2016.

791    Twomey, S.: The influence of pollution on the shortwave albedo of clouds, J. Atmos. Sci., 34, 1149–1152, 1977.

792    UNEP/WMO: Integrated Assessment of Black Carbon and Tropospheric Ozone, Nairobi, Kenya, available at:
793        http://wedocs.unep.org/handle/20.500.11822/8028 (last access: 13 May 2020), 2011.

794    US EPA: Guidance on the use of models and other analyses for demonstrating attainment of air quality goals for
795        ozone, PM$_{2.5}$, and regional haze. U.S. Environmental Protection Agency Office of Air Quality Planning and
796        Standards Air Quality Analysis Division Air Quality Modeling Group Research Triangle Park, NC, 2007.
797    Zhang, H. Y., Cheng, S. Y., Yao, S., Wang, X. Q., and Zhang, J. F.: Multiple perspectives for modeling regional PM$_{2.5}$
798        transport across cities in the Beijing–Tianjin–Hebei region during haze episodes, Atmos. Environ., 212, 22–35,
799        https://doi.org/10.1016/j.atmosenv.2019.05.031, 2019.
800    Zhang, X., Zhang, Y. H, Han, J. B., Zhang, L., and Shi, W. R.: Analysis of the climatic characteristics of the
801        atmospheric boundary layer height in yanmayan Island, Arctic (in Chinese), Polar studies, 30(02):132–139, 2018.